

# On the relationship between parameters and discharge data for a lumped karst aquifer model

<sup>1</sup>Chair of Hydrology and River Basin Management, Technical University of Munich, Arcisstr. 21, 80333 Munich, Germany

<sup>2</sup>Chair for Numerical Mathematics, Technical University of Munich, Boltzmannstrae 3, 85748 Garching, Germany

<sup>3</sup>Institute of Geography, University of Innsbruck, Innrain 52, 6020 Innsbruck, Austria

**Daniel Bittner<sup>1</sup>, Mario Teixeira Parente<sup>2</sup>, Steven Mattis<sup>2</sup>, Barbara Wohlmuth<sup>2,3</sup>, and Gabriele Chiogna<sup>1,4</sup>**

## Key Points:

- = Hydrotype parameters in the LuKARS model are similarly informed by data
- = All 21 calibration parameters are informed by the data
- = Not possible to apply any model reduction scheme for LuKARS

## Abstract

Hydrological models of karst aquifers are generally semi distributed and physical processes such as infiltration and spring discharge generation are described in a lumped way. Several works previously addressed the problems associated with the calibration of such models, highlighting in particular the issue of model equifinality and the importance of multi-objective optimization. In this work, we investigate the problem of model calibration from a different point of view. We apply the active subspace method, to investigate how the parameters of a newly proposed hydrological model for karst aquifers (LuKARS, Land use change modeling in KARSt systems) are informed by discharge data. We showed that each one of the three hydrotopes (i.e. distinct landscape units characterized by homogeneous hydrological properties as a result of similar land use and soil types) used in the model are similarly informed by the data. We found that all the 21 model parameters are informed by the measured data and therefore it is not immediately possible to apply any model reduction scheme. The full-dimensional inverse problem is formulated and solved to identify local optima for the misfit function.

## 1 Introduction

Parameter calibration is a fundamental step to be performed before applying any hydrological model (Beven & Binley, 1992). A large amount of literature describes several different methods to estimate model parameters (Tarantola, 2005; Aster et al., 2011; Kitanidis & Lee, 2014). A specific challenge for hydrological models, is the large dimensionality of the parameter space, i.e., the amount of independent parameters that need to be estimated using inverse modeling is large. Moreover, it is difficult to quantify how and which model parameters are informed by the measurements used to calibrate the model.

A recently developed method, called the active subspace method (P. G. Constantine et al., 2014a), when applied to inverse problems identifies directions in parameter space that are most informed by data. The active subspace method has been successfully applied to different contexts (P. G. Constantine et al., 2015; Teixeira Parente et al., 2018), including a hydrological model by Jefferson, Gilbert, Constantine, and Maxwell (2015). To the best of our knowledge, a previous application to a lumped rainfall-discharge model for karstic systems does not exist, but it is valuable since most of the lumped parameters are not measurable and, hence, it is difficult to quantify how the measurements used for model calibration inform the model parameters.

Due to the complex interaction between surface, fracture and conduit flows, karst catchments are highly complex systems and very little information is generally available about the subsurface geological structures. Model predictions about spring discharge are therefore affected by significant uncertainties (Chen et al., 2018; Henson et al., 2018). The lack of spatial distributed information about subsurface flow in karst systems makes conceptual rainfall-discharge models appreciable tools to predict karst spring discharge, since they allow to drastically simplify the description of the functioning of the subsurface system (Hosseini et al., 2017). However, finding a suitable model representation is not trivial since it is difficult to constrain the model parameter range according to field observations and measurements. The general trade-off to be made is two-fold: i) a severe simplification of a complex karst system may lead to an underrepresentation of dominant processes and, thus, to model prediction uncertainties. However, keeping the parameter space low-dimensional, i.e. 4 to 6 parameters (Jakeman & Hornberger, 1993), may reduce parameter uncertainties and model equifinality (Beven, 2006); ii) making the conceptual model more complex and accounting for a more detailed representation of the hydrological processes (e.g. when considering land use change impacts in karst systems) can increase the model uncertainty and equifinality (Hartmann et al., 2014). Con-

sidering more complexity in the modeling framework, however, can improve the conceptual representation of the regarded karst system (Hartmann, 2018).

Most applied karst rainfall-discharge models use a minimum of 6 parameters (Hartmann et al., 2017). Their sensitivity and the identification of the parameters which are informed by the observations used for model calibration is a primary concern for the community dealing with karst modeling. Different approaches were recently proposed to reduce model structure and parameter uncertainties for rainfall-discharge models applied in karst hydrology. Hartmann, Barberá, Lange, Andreo, and Weiler (2013) developed an evaluation strategy to identify the most valid model structure while finding a balance between an appropriate model structure, parameter estimation and model performance for a karst system of interest. Moreover, Hartmann et al. (2017) presented an approach to consider hydrochemical data to constrain parameter ranges of the VarKarst model (Hartmann, Wagener, et al., 2013). Further multi-objective calibration frameworks were proposed by Moussu, Oudin, Plagnes, Mangin, and Bendjoudi (2011) and Mazzilli et al. (2013); the first research study calibrated two rainfall-discharge models with respect to the match of the observed and the simulated discharge time series and the autocorrelation of the discharge, the second one further used ground-based gravity measurements to consider the matrix water storage in the model calibration process. An analytic approach is then needed to perform a global sensitivity analysis of the full parameter space and to investigate the reducibility of the parameter dimensions to ensure that each applied parameter is equally informed.

In this work, we perform active subspace analysis on the recently proposed hydrootope-based LuKARS model (Bittner et al., 2018) for the Kerschbaum spring recharge, in Austria. Hydrotopes are distinct landscape units characterized by homogeneous hydrological properties as a result of similar land use and soil types (Koeck & Hochbichler, 2012) and are used to include in the model the effect of land use change in model predictions. We investigate how model parameters are informed by karst spring discharge observations using a rainfall-discharge model with a 21-dimensional parameter space and we try to identify an optimal set of parameters that minimize the difference between model prediction and spring discharge measurements.

## 2 Case study

Our case study is the Kerschbaum karst springshed located 10km south of Waidhofen a.d. Ybbs (Austria) (Fig. 1a). On a regional scale, this pre-alpine catchment is part of the eastern foothills of the Northern Calcareous Alps with altitudes ranging between 415m and 969m a.s.l. The area is further characterized by a warm-moderate regional climate with a mean annual temperature of 8°C and a mean annual precipitation of 1379mm. The annual distribution of the precipitation is bimodal with maxima during the summer (June and July) and winter periods (December and January), being indicative for the relevance of rainfall and snowfall-related processes in the study area (Bittner et al., 2018).

Several spring outlets exist in the study area of which some are used for the local water supply of the community of Waidhofen a.d. Ybbs. Here, the Kerschbaum spring represents the most important one with a mean annual discharge of 34ls<sup>-1</sup>. Prior hydrogeological investigations revealed that the Kerschbaum spring is fed by the karst aquifer of the dolomitic bedrock (Hacker, 2003), which is part of the Triassic Main Dolomite strata of the Northern Calcareous Alps. The small-scale recharge area comprises a surface area of 2.5km<sup>2</sup> and is predominantly covered by beech forests. Four major hydrotopes ((Arnold et al., 1998)), i.e., distinct landscape units characterized by homogeneous hydrological properties as a result of similar land use and soil types are present. Today, about 7% of the recharge area are used for dolomite mining activities, represented by hydrotope Hyd Q in Fig. 1b). Three more hydrotopes were classified in the recharge area, which are Hyd

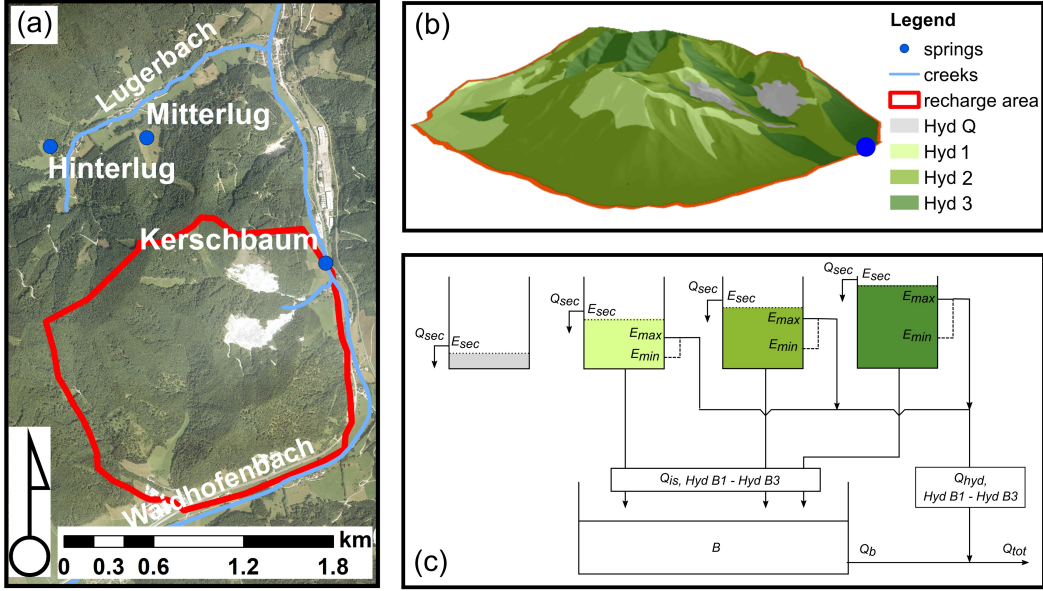


**Figure 1.** Overview of the study area Waidhofen a.d. Ybbs (Austria) and the the conceptualization of the Kerschbaum spring recharge area. (a) The location and the boundary of the Kerschbaum spring recharge area in the study area. The orthophoto shows that the predominant landcover is forest. (b) Pseudo-3-dimensional view on the topography of the Kerschbaum recharge area including the hydrotope classification according to Koeck and Hochbichler (2012). (c) Conceptual model of the recharge area as implemented in LuKARS, considering each hydrotope as a distinct storage unit. The different sizes of the tanks show the different storage capacities of the respective hydrotopes (not to scale).

1, Hyd 2 and Hyd 3 (shown in Fig. 1b) and are named after their dominant land cover according to Koeck and Hochbichler (2012). Hyd 1 (*Bluegrass-Beech Forest hydrotope*) is characterized by shallow and coarse-grained soils, being indicative for a low storage capacity. Hyd 2 (*White Sedge-Beech Forest hydrotope*) has more fined grained soils with moderate thicknesses. Finally, Hyd 3 (*Christmas Rose-Beech Forest hydrotope*) is dominated by mostly loam textured soils with more elevated thicknesses and has the highest storage capacity as compared to Hyd 1 and Hyd 2. A more detailed description of the study area and the hydrotopes can be found in Bittner et al. (2018) and Sheikhy Narany, Bittner, Disse, and Chiogna (2018).

### 3 Methods

#### 3.1 LuKARS model

The LuKARS rainfall-discharge model we investigated was recently introduced by Bittner et al. (2018). The general idea of the modeling approach is to perform land use change impact studies in a karstic environment by implementing it in areas with homogeneous infiltration conditions as distinct hydrological response units, the hydrotopes. The core of the LuKARS model is a non-linear hysteretic transfer function (Tritz et al., 2011) based on which each hydrotope is implemented. Conceptually, a hydrotope represents a tank that controls the quickflow component (conduit flow,  $Q_{hyd,i}$ ) and the recharge of a given response unit ( $Q_{is,i}$ ) in a recharge area of interest. All hydrotopes transfer a certain amount of discharge to a joint baseflow storage, which is fed by each hydrotope

individually. The baseflow storage then controls the baseflow contribution ( $Q_b$ ) to the spring by a linear transfer function. The non-linear quickflow initiates once a hydrootope-specific storage threshold was reached. Then, this fastflow component is directly moved to the spring outlet and bypasses the baseflow storage.

The hydrootope implementation is based on the classification of similar soil and land use areas within a the catchment and most parameters in LuKARS cannot be derived by field measurements. The parameter sets to describe the storage and discharge behavior of a hydrootope cannot be considered completely independent between different hydrotopes, since they must reflect the differences in the hydrological response of different soils and land use. For example, a given parameter set of a hydrootope with a small storage volume (e.g. a shallow, coarse-grained soil like Hyd 1 in Fig. 1b) and c) needs to be interpreted in relation to the parameters applied to a second hydrootope with a higher storage volume (e.g. a thicker, more fine-grained soil like Hyd 3 in Fig. 1b) and c). The physical constraints about the ranking of the hydrootope parameters are provided in 3.3.

It is important to note, that the conceptual character of LuKARS and the large number of calibration parameters make this approach prone to model uncertainties and constrain its applicability for the prediction of karst water resources. Thus, there is a general need to investigate the informativeness of each single parameter, as well as to quantify parameter uncertainty. A deeper understanding of the way how model parameters are informed by date can significantly improve the reliability of water resources predictions with LuKARS.

A detailed description of the modeling approach including the system of equations of LuKARS is presented in Appendix A.

### 3.2 Identification of the parameters informed during inverse modeling

In order to identify the parameters which are informed by the data used for model calibration, we use the *active subspaces* method. *Active subspaces* is a recently developed method for dimension reduction (P. Constantine & Gleich, 2014; P. G. Constantine, 2015; P. G. Constantine et al., 2014b) which identifies important directions in the parameter space. It has been shown to be useful in several applications including approximation, integration, optimization, and sensitivity analysis (P. G. Constantine, 2015). Recently, active subspaces have been used to reduce the dimension of parameter spaces in inverse problems (P. G. Constantine et al., 2016; Cortesi et al., 2017; Teixeira Pariente et al., 2018).

We now summarize the basic theory of active subspaces for inverse problems. We consider the situation in which  $\mathbf{d}$  represents the observed time series, that we aim at modeling (e.g., spring discharge in our case). Then, the map  $\mathcal{G}$  represents our forward LuKARS model run with a given set of input parameter  $\mathbf{x}$ . Finally, we consider  $\boldsymbol{\eta} \sim \mathcal{N}(\mathbf{0}, \Gamma)$  a zero-centered Gaussian noise with covariance  $\Gamma$ , such that:

$$\mathbf{d} = \mathcal{G}(\mathbf{x}) + \boldsymbol{\eta}, \quad (1)$$

The unregularized cost function for inversion and uncertainty quantification of this problem is the data misfit function

$$f_{\mathbf{d}}(\mathbf{x}) := \frac{\|\mathbf{d} - \mathcal{G}(\mathbf{x})\|_{\Gamma}}{2} := \frac{\|\Gamma^{-1/2}(\mathbf{d} - \mathcal{G}(\mathbf{x}))\|_2}{2} \quad (2)$$

The classical inverse problem to determine the parameters that best match the data is

$$\mathbf{x}^* = \min_{\mathbf{x} \in \mathcal{X}} f_{\mathbf{d}}(\mathbf{x}), \quad (3)$$

i.e. to find the parameters that minimize the data misfit. Importantly, the solution to the inverse problem (3) is generally not unique.

To identify important directions of a function of interest (in our case the misfit function), one looks at eigenpairs of the positive semi-definite  $n \times n$  matrix

$$\mathbf{C} := \int \nabla f(\mathbf{x}) \nabla f(\mathbf{x})^\top \rho(\mathbf{x}) d\mathbf{x} = \mathbf{W} \Lambda \mathbf{W}^\top, \quad (4)$$

where  $n$  is the number of model parameters,  $\rho$  is a given prior probability density function, and  $f$  is continuous and differentiable on the support of  $\rho$  and has square-integrable derivatives with respect to  $\rho$ . For the given inversion,  $f$  is the data misfit function  $f_d$ . If there is a large gap in the eigenvalue decay, it indicates that there are directions in the space of unknown parameters where  $f_d$  varies much more on average than other directions, i.e. these directions are significantly more informed by the data. The directions corresponding with the eigenvectors associated with the significant eigenvalues is called the *active subspace*. If an active subspace is identified it can be used to effectively reduce the dimension of the parameter space for inversion, potentially greatly reducing the computational cost. It also tells you that not all directions are well-informed by the data, so new data to which these directions are sensitive would be needed to accurately estimate parameters in this *inactive subspace*.

$\mathbf{C}$  can be approximated by Monte Carlo integration:

$$\mathbf{C} \approx \frac{1}{N} \sum_{j=1}^N \nabla f(\mathbf{x}_j) \nabla f(\mathbf{x}_j)^\top = \mathbf{W} \Lambda \mathbf{W}^\top \quad (5)$$

for samples  $\mathbf{x}_j$  distributed according to  $\rho$ . A relatively small number of samples (in our case about 250) is required to calculate an approximation of  $\mathbf{C}$  with the proper significant eigenvalues (see P. G. Constantine et al. (2015)). Gradients can be calculated by using methods such as adjoint approaches, finite differences and radial basis functions.

If there is a large enough spectral gap after the  $k$ th eigenvalue of  $\mathbf{C}$ , one can define a corresponding  $k$ -dimensional active subspace and variables on it. With enough samples in the Monte Carlo approximation of  $\mathbf{C}$ , a larger spectral gap leads to a more accurate approximation of the active subspace (P. Constantine & Gleich, 2014). The approximation quality of the active subspace can be estimated by using *bootstrap intervals*. We regard the quality of approximation in terms of *subspace estimation errors*. For algorithmic details, i.e. how to compute the subspace errors, see P. Constantine and Gleich (2014); P. G. Constantine (2015).

### 3.3 Relation between model and calibration parameters

The *model parameters* for hydrotope  $i$  described in Table 1 are  $k_{hyd,i}$  (discharge parameter for  $Q_{hyd,i}$ ),  $E_{min,i}$  (minimum storage capacity Hyd  $i$ ),  $E_{max,i}$  (maximum storage capacity Hyd  $i$ ),  $\alpha_i$  (quickflow exponent of Hyd  $i$ ),  $k_{is,i}$  (discharge parameter for  $Q_{is,i}$ ),  $k_{sec,i}$  (discharge parameter for  $Q_{sec,i}$ ),  $E_{sec,i}$  (activation level for  $Q_{sec,i}$ ), where the index  $i = 1, 2, 3$  indicates the different hydrotopes.

Since the model parameters for each hydrotope have to meet some ranking constraints as described in 3.1, they are not independent from a statistical point of view. However, the active subspace framework prefers independent parameters which leads to the introduction of artificial parameters. It is worth distinguishing between the 7 aforementioned model parameters for each hydrotope and the related calibration parameters described in the following.

We need to introduce two types of artificial parameters.

1) Since  $E_{min,i} \leq E_{max,i}$ , we set  $E_{max,i} := E_{min,i} + \Delta e_i$ ,  $i = 1, 2, 3$ , for new calibration parameters  $\Delta e_i$ .

**Table 1.** Overview of the model parameters, their physical units and descriptions and the prior intervals used for the active subspace method.

Parameter	unit	description	lower bound	upper bound
$k_{hyd,1}$	$[L^2 T^{-1}]$	discharge parameter for $Q_{hyd,1}$	9	900
$E_{min,1}$	[L]	minimum storage capacity Hyd 1	10	50
$E_{max,1}$	[L]	maximum storage capacity Hyd 1	15	75
$\alpha_1$	[·]	quickflow exponent of Hyd 1	0.7	1.6
$k_{is,1}$	$[LT^{-1}]$	discharge parameter for $Q_{is,1}$	0.002	0.2
$k_{sec,1}$	$[LT^{-1}]$	discharge parameter for $Q_{sec,1}$	0.0095	0.95
$E_{sec,1}$	[L]	activation level for $Q_{sec,1}$	25	70
$k_{hyd,2}$	$[L^2 T^{-1}]$	discharge parameter for $Q_{hyd,2}$	8.5	850
$E_{min,2}$	[L]	minimum storage capacity Hyd 2	40	80
$E_{max,2}$	[L]	maximum storage capacity Hyd 2	80	160
$\alpha_2$	[·]	quickflow exponent of Hyd 2	0.5	1.3
$k_{is,2}$	$[LT^{-1}]$	discharge parameter for $Q_{is,2}$	0.00055	0.055
$k_{sec,2}$	$[LT^{-1}]$	discharge parameter for $Q_{sec,2}$	0.0023	0.23
$E_{sec,2}$	[L]	activation level for $Q_{sec,2}$	130	220
$k_{hyd,3}$	$[L^2 T^{-1}]$	discharge parameter for $Q_{hyd,3}$	7.7	770
$E_{min,3}$	[L]	minimum storage capacity Hyd 3	70	120
$E_{max,3}$	[L]	maximum storage capacity Hyd 3	155	255
$\alpha_3$	[·]	quickflow exponent of Hyd 3	0.2	0.7
$k_{is,3}$	$[LT^{-1}]$	discharge parameter for $Q_{is,3}$	0.00025	0.025
$k_{sec,3}$	$[LT^{-1}]$	discharge parameter for $Q_{sec,3}$	0.0015	0.15
$E_{sec,3}$	[L]	activation level for $Q_{sec,3}$	320	450

2) The physical constraints for the model parameters are (Bittner et al., 2018):

$$k_{hyd,1} \geq k_{hyd,2} \geq k_{hyd,3}, \quad (6)$$

$$E_{min,1} \leq E_{min,2} \leq E_{min,3}, \quad (7)$$

$$\alpha_1 \geq \alpha_2 \geq \alpha_3, \quad (8)$$

$$k_{is,1} \geq k_{is,2} \geq k_{is,3}, \quad (9)$$

$$k_{sec,1} \geq k_{sec,2} \geq k_{sec,3}, \quad (10)$$

$$E_{sec,1} \leq E_{sec,2} \leq E_{sec,3}. \quad (11)$$

We introduce new calibration parameters that mimic the difference between values of two successive hydrotopes. We make sure that the physical parameter constraints are met and that values are chosen such that the corresponding model parameters lie in the respective specified intervals.

In particular, we set for  $i = 2, 3$

$$k_{hyd,i} := k_{hyd,i,lb} + \Delta k_{hyd,(i-1,i)} (\min \{k_{hyd,i,ub}, k_{hyd,i-1}\} - k_{hyd,i,lb}), \quad (12)$$

$$E_{min,i} := \max \{E_{min,i-1}, E_{min,i,lb}\} + \Delta E_{min,(i-1,i)} (E_{min,i,ub} - \max \{E_{min,i-1}, E_{min,i,lb}\}), \quad (13)$$

$$\alpha_i := \alpha_{i,lb} + \Delta \alpha_{(i-1,i)} (\min \{\alpha_{i,ub}, \alpha_{i-1}\} - \alpha_{i,lb}), \quad (14)$$

$$k_{is,i} := k_{is,i,lb} + \Delta k_{is,(i-1,i)} (\min \{k_{is,i,ub}, k_{is,i-1}\} - k_{is,i,lb}), \quad (15)$$

$$k_{sec,i} := k_{sec,i,lb} + \Delta k_{sec,(i-1,i)} (\min \{k_{sec,i,ub}, k_{sec,i-1}\} - k_{sec,i,lb}), \quad (16)$$

$$E_{sec,i} := \max \{E_{sec,i-1}, E_{sec,i,lb}\} + \Delta E_{sec,(i-1,i)} (E_{sec,i,ub} - \max \{E_{sec,i-1}, E_{sec,i,lb}\}), \quad (17)$$

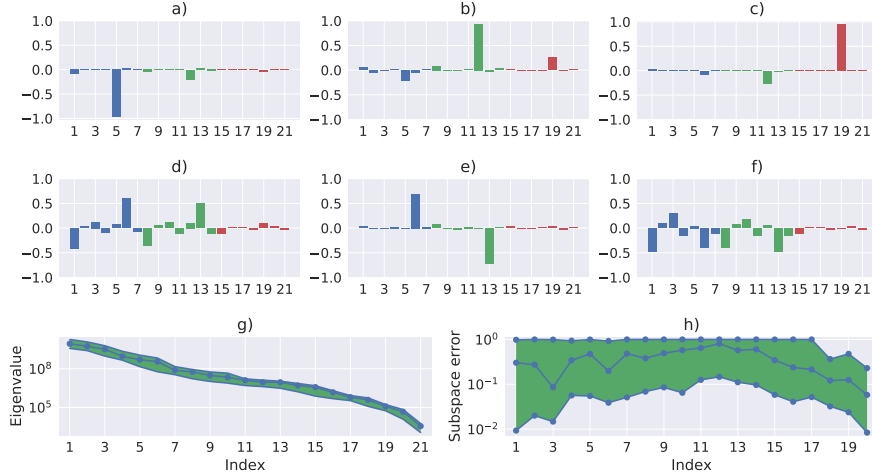


**Figure 2.** Results of the active subspace method applied to LuKARS. a) - f) show the first six eigenvectors of the 21-dimensional parameter space, g) the eigenvalue decay related to each eigenvector and h) the subspace error of the eigenvectors.

where lower and upper bounds of each interval for the model parameters are denoted by subscripts  $_{lb}$  and  $_{ub}$ , respectively. This results in a 21-dimensional vector of calibration parameters, i.e.

$$\begin{aligned} \boldsymbol{x} := & (k_{\text{hyd},1}, E_{\text{min},1}, \Delta e_1, \alpha_1, k_{\text{is},1}, k_{\text{sec},1}, \\ & \Delta k_{\text{hyd},(1,2)}, \Delta E_{\text{min},(1,2)}, \Delta e_2, \Delta \alpha_{(1,2)}, \Delta k_{\text{is},(1,2)}, \Delta k_{\text{sec},(1,2)}, \Delta E_{\text{sec},(1,2)}, \\ & \Delta k_{\text{hyd},(2,3)}, \Delta E_{\text{min},(2,3)}, \Delta e_3, \Delta \alpha_{(2,3)}, \Delta k_{\text{is},(2,3)}, \Delta k_{\text{sec},(2,3)}, \Delta E_{\text{sec},(2,3)})^\top \in \mathbb{R}^{21}. \end{aligned} \quad (18)$$

All the eigenvalues and eigenvectors that are shown in Section 4 refer to this vector of calibration parameters.

## 4 Results and discussion

In Figs 2a) - f) we show the first six (out of 21) eigenvectors obtained using the active subspace method. The 21 components of each vector, represent the 21 components of the calibration parameter vector  $\vec{x}$  (Eq. 18). The model parameters associated to each component of the calibration parameter vector  $\vec{x}$  are indicated in Table 1. Each hydrotope is characterized by 7 independent parameters. Therefore, the components 1-7 are inherent to Hyd 1, the components 8-14 represent Hyd 2 and the components 15-21 Hyd 3. We can observe that the rank order of the absolute values of the components of the eigenvectors associated to the parameters of each hydrotope follow a very similar pattern.

For example, in the first eigenvector (Fig. 2a), the largest components (taken as absolute value) are number 5, number 12 and number 19, for hydrotope 1, 2 and 3, respectively. They are associated with  $k_{is}$  for each hydrotope. Moreover, the first three eigenvectors (Figs. 2a) - c) show that the calibration parameters associated with  $k_{is}$  display the largest components (taken as absolute value), for hydrotope 1, 2 and 3, respectively. Also considering the eigenvectors 3 to 6, shown in Figs. 2d) -f), respectively, we can observe a marked similarity, in particular between Hyd 1 and Hyd 2, while Hyd 3 displays a slightly weaker similarity although the general pattern in the rank order of

**Table 2.** Best model parameters for the calibration period from 01/01/2006 to 31/12/2008 found with the Nelder-Mead simplex algorithm.

Hydrotope	$k_{hyd}$	$E_{min}$	$E_{max}$	$\alpha$	$k_{is}$	$k_{sec}$	$E_{sec}$
Hyd 1	269.7	15.3	23.9	0.92	0.12	0.81	51.0
Hyd 2	80.1	40.7	102.3	0.66	0.0036	0.02	174.7
Hyd 3	61.4	110.1	214.5	0.5	0.0028	0.013	372.2

the parameters is maintained. This is due to the fact that Hyd 3 has a much more homogeneous hydrological response than Hyd 1 and Hyd 2, and therefore the discharge data are not able to inform its parameters as much as Hyd 1 and Hyd 2. From a hydrological point of view, Hyd 3 has the highest storage capacity and the most fine-grained soil texture, leading to a better water retention capacity. This causes that the discharge processes originating from Hyd 3, i.e.  $Q_{hyd}$  and  $Q_{is}$ , are weakened and more homogeneous as compared to Hyd 1 and Hyd 2. The strong similarity between the way how different calibration parameters are similarly informed by spring discharge data is indicative about the robustness of the hydrotope approach. It highlights that, although the model is lumped and not physically based, the hydrotopes parameters can be similarly inferred by discharge observation.

It is important to observe that the results obtained using the active subspace method are not equivalent to a standard global or local sensitivity analysis. The fact that the calibration parameters associated with  $k_{is}$  are informed by the data in all three hydrotopes and they have the largest components does not necessarily imply that they are the most sensitive parameters (i.e., it is not necessarily true that small variations in the value of  $k_{is}$  lead to large variations in the misfit function). What the analysis of the eigenvector tells us, is that, if we started with a very large range for the calibration of  $k_{is}$ , then we would be able to better constrain the value of this parameter, given the spring discharge observations that we use for model calibration. Fig. 2g) shows the decay in the eigenvalues associated to each eigenvector, along with the minimum and maximum estimated eigenvalue. The active subspace method often discovers a spectral gap, i.e., an abrupt decrease in the eigenvalues. This is not the case for the LuKARS model. One could judge as sufficient the decrease in the eigenvalues observed after eigenvector 3 (from an eigenvalue of  $3.2 \times 10^9$  to an eigenvalue of  $9.0 \times 10^8$ ) or 6 (from an eigenvalue of  $3.5 \times 10^8$  to an eigenvalue of  $7.6 \times 10^7$ ). In fact, as indicated in Fig. 2h), also the subspace error displays a drop at eigenvectors 3 and 6. However, we have a very large uncertainty in its estimation, excluding the usage of a reduced dimension approach. As a practical implication, this means that we cannot exclude any of the eigenvectors during model calibration. All calibration parameters are informed by the data and play a significant role for the calibration. Although the active subspace method is generally applied to achieve an efficient model reduction, and hence to decrease the computational cost of solving the inverse problem, in this case it is used to show that actually such an approach cannot be followed.

For the solution of the full-dimensional inverse problem, we used the Nelder-Mead simplex algorithm. Despite it does not have a fast convergence rate and it does not guarantee the identification of a global optimum, it is a robust method that does not rely on any highly limiting assumption for its application. A drawback of using the Nelder-Mead simplex algorithm is that to explore the 21 dimensional parameter space in order to verify how much the optimal set of parameters identified by the optimization depends on the starting point of the algorithm. In order to overcome this issue, we ran a set of 2100 independent simulations (i.e., with different starting points) to investigate if different sets

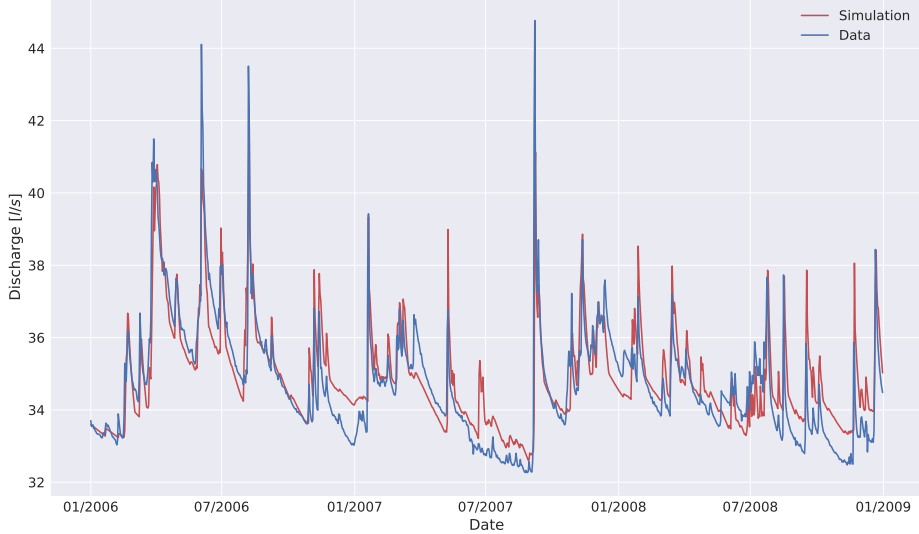


**Figure 3.** Simulation results obtained with the best parameter set obtained by Nelder-Mead simplex algorithm for the calibration period from 01/01/2006 to 31/12/2008.

of parameters can lead to similar values of the misfit function (i.e., model equifinality). The results indicate that the calibration parameters with the largest magnitude (in absolute value) in the three most important eigenvectors (parameters associated with  $k_{is}$  for all hydrotopes) converge to very similar model parameter values as for the best parameter set ( $k_{is,1} = 0.1$ ,  $k_{is,2} = 0.004$ ,  $k_{is,3} = 0.003$ ) if we consider the best 100 realizations, ranked according to the minimum misfit value. The repeated occurrence of a single value for the parameters associated with  $k_{is}$  for all hydrotopes indicates that they are well informed by the discharge data. Since the subsequent eigenvectors display eigenvalues at least one order of magnitude smaller than the first three, also the calibrated parameters occurring as important components are less informed by the data. Other common optimization methods were also tested but were not as effective. The best parameter set obtained using the optimization algorithm is provided in Table 2 and the results are displayed in Fig. 3. With this parameter set it was possible to obtain a misfit value of 9.9. The parameter set was then applied for a one-year validation period and the obtained misfit value was 9.2.

## 5 Conclusion

In the presented research, we applied the active subspace method to the LuKARS rainfall-discharge model (Bittner et al., 2018) to investigate how much each parameter of the model is informed by the discharge data and if the parameter dimensions of the model can be reduced. Our results for the Kerschbaum spring case study (21 parameter dimensions) showed that no significant active subspace could be found in the 21-dimensional parameter space. No dimension reduction is possible in the LuKARS model, indicating the importance of each individual parameter in the model calibration process. The implemented hydrotopes were similarly informed by the discharge data, which highlights the robustness of the hydrotope-based approach for hydrological modeling in karst systems.

After running 2100 independent simulations using the Nelder-Mead simplex algorithm, we found that the discharge coefficients  $k_{is}$  converged to similar model parameter values when comparing the parameter values of the best 100 simulations (in terms of lowest data misfit). These parameters relate to the most important eigenvectors with the largest magnitude (in absolute values) found with the active subspace method, showing that the prior distribution of the most informed parameters could significantly be constrained. Nevertheless, we need to find other applicable methods to further reduce model equifinality with respect to the other calibration parameters of LuKARS. Additionally, our future efforts will further focus on investigating practicable methods for the uncertainty quantification of lumped and semi-distributed karst rainfall-discharge models with high parameter dimensions.

## A The LuKARS model

In the following, we describe the system of equations of the LuKARS model (Bittner et al., 2018). The  $i$  subscript notation specifies that the respective terms are hydrootope specific. LuKARS solves the following balance equation for each hydrootope:

$$\frac{dE_i}{dt} = \begin{cases} S_x - \frac{Q_{sec,i} + Q_{is,i} + Q_{hyd,i}}{a_i} & \text{if } E_i > 0 \\ 0 & \text{if } E_i = 0 \end{cases} \quad (\text{A.1})$$

$E_i$  indicates the water level [L] in hydrootope  $i$ ,  $t$  [T] is the time and  $S_i$  is the hydrootope-specific sink and source term as a mass balance of precipitation, snow melt, evapotranspiration and interception.  $Q_{sec}$  [ $L^3 T^{-1}$ ] integrates all flow components that do not arrive at the investigated karst spring and that are transferred outside the regarded recharge area, i.e. secondary spring discharge and overland flow.  $Q_{is,i}$  [ $L^3 T^{-1}$ ] represents the discharge from hydrootope  $i$  to the underlying baseflow storage, being the conceptual representation for the process of groundwater recharge.  $Q_{hyd,i}$  [ $L^3 T^{-1}$ ] is considered a hydrootope-specific quickflow component occurring in preferential flow paths (e.g. subsurface conduits) that is directly transferred to the spring outlet and is responsible for the fast reaction of a spring discharge to rainfall and snowmelt events. The absolute area covered by a respective hydrootope is given by  $a_i$  [ $L^2$ ].

The model solves the following balance equation for the baseflow storage:

$$\frac{dE_b}{dt} = \begin{cases} \frac{\Sigma(Q_{is,i}) + Q_b}{A} & \text{if } E_b > 0 \\ 0 & \text{if } E_b = 0 \end{cases} \quad (\text{A.2})$$

where  $E_b$  indicates the water level [L] in the baseflow storage and  $\Sigma(Q_{is,i})$  [ $L^3 T^{-1}$ ] are the cumulative flows from all hydrotopes to the baseflow storage.  $Q_b$  [ $L^3 T^{-1}$ ] represents water that is transferred from the storage B to the spring and simulates a baseflow contribution from the phreatic aquifer system to the spring discharge. The variable  $A$  [ $L^2$ ] stands for the entire recharge area. The discretized forms of A.1 and A.2, as given in A.3 and A.4, are solved for each time step  $n$ :

$$E_{i,n+1} = \max[0, E_{i,n} + (S_{i,n} - \frac{Q_{sec,i,n} + Q_{is,i,n} + Q_{hyd,i,n}}{a_i}) * \Delta t] \quad (\text{A.3})$$

$$E_{b,n+1} = \max[0, E_{b,n} + (\frac{\Sigma(Q_{is,i,n}) - Q_{b,n}}{A}) * \Delta t] \quad (\text{A.4})$$

The discharge terms are computed as follows:

$$Q_{hyd,i,n} = \varepsilon \left[ \frac{\max(0, E_{i,n} - E_{min,i})}{E_{max,i} - E_{min,i}} \right]^\alpha * \frac{k_{hyd,i}}{l_{hyd,i}} * a_i \quad (\text{A.5})$$

$$Q_{is,i,n} = k_{is,i} * E_{i,n} * a_i \quad (\text{A.6})$$

$$Q_{sec,i,n} = k_{sec,i} * \max(0, E_{i,n} - E_{sec,i}) * a_i \quad (\text{A.7})$$

$$Q_{b,n} = k_b * E_{b,n} * A \quad (\text{A.8})$$

$E_{max,i}$  [L] and  $E_{min,i}$  [L] represent the upper and lower storage thresholds of the hydrotope  $i$ .  $E_{sec,i}$  [L] is the hydrotope-specific activation level for a secondary spring discharge.  $k_{is,i}$  [ $\text{LT}^{-1}$ ] and  $k_{sec,i}$  [ $\text{LT}^{-1}$ ] are the specific discharge parameters for  $Q_{is,i}$  [ $\text{L}^3\text{T}^{-1}$ ] and  $Q_{sec,i}$  [ $\text{L}^3\text{T}^{-1}$ ], respectively.  $k_{hyd,i}$  [ $\text{L}^2\text{T}^{-1}$ ] represents the specific discharge parameter for the quickflow of a hydrotope and  $l_{hyd,i}$  [L] is the mean distance of hydrotope  $i$  to the adjacent spring, thus accounting for the relative location of the same hydrotope types in a specific recharge area. The ratio between  $k_{hyd,i}$  and  $l_{hyd,i}$  represents the hydrotope discharge coefficient. The dimensionless connectivity/activation indicator  $\varepsilon$  is defined as follows:

$$\varepsilon_{n+1} = 0 \text{ if } \begin{cases} \varepsilon_n = 0 \text{ \& } E_{i,n+1} < E_{max,i} \text{ or} \\ \varepsilon_n = 1 \text{ \& } E_{i,n+1} \leq E_{min,i} \end{cases} \quad (\text{A.9})$$

$$\varepsilon_{n+1} = 1 \text{ if } \begin{cases} \varepsilon_n = 0 \text{ \& } E_{i,n+1} \geq E_{max,i} \text{ or} \\ \varepsilon_n = 1 \text{ \& } E_{i,n+1} > E_{min,i} \end{cases} \quad (\text{A.10})$$

### Acknowledgments

This collaborative research is a result of the UNMIX project (Uncertainties due to boundary conditions in predicting mixing in groundwater), which is funded by the IGSSE (International Graduate School of Science and Engineering) of the Technical University of Munich. The authors further thank the water works Waidhofen a.d. Ybbs for providing the relevant spatial and time series data.

## References

Arnold, J. G., Srinivasan, R., Muttiah, R. S., & Williams, J. R. (1998). Large area hydrologic modeling and assessment part i: model development 1. *JAWRA Journal of the American Water Resources Association*, 34(1), 73–89.

Aster, R. C., Borchers, B., & Thurber, C. H. (2011). *Parameter estimation and inverse problems* (Vol. 90). Academic Press.

Beven, K. (2006). A manifesto for the equifinality thesis. *Journal of Hydrology*, 320(1-2), 18–36. doi: 10.1016/j.jhydrol.2005.07.007

Beven, K., & Binley, A. (1992). The future of distributed models: model calibration and uncertainty prediction. *Hydrological processes*, 6(3), 279–298.

Bittner, D., Sheikhy Narany, T., Kohl, B., Disse, M., & Chiogna, G. (2018). Modeling the hydrological impact of land use change in a dolomite-dominated karst system. *Journal of Hydrology*(under review).

Chen, Z., Hartmann, A., Wagener, T., & Goldscheider, N. (2018). Dynamics of water fluxes and storages in an alpine karst catchment under current and potential future climate conditions. *Hydrology and Earth System Sciences*, 22(7), 3807–3823. doi: 10.5194/hess-22-3807-2018

Constantine, P., & Gleich, D. (2014). Computing active subspaces with Monte Carlo. *arXiv preprint arXiv:1408.0545*.

Constantine, P. G. (2015). *Active Subspaces* (Vol. 2). Society for Industrial and Applied Mathematics (SIAM), Philadelphia, PA. (Emerging Ideas for Dimension Reduction in Parameter Studies)

Constantine, P. G., Dow, E., & Wang, Q. (2014a). Active subspace methods in theory and practice: Applications to kriging surfaces. *SIAM Journal on Scientific Computing*, 36(4), A1500–A1524. doi: 10.1137/130916138

Constantine, P. G., Dow, E., & Wang, Q. (2014b). Active subspace methods in theory and practice: applications to kriging surfaces. *SIAM J. Sci. Comput.*, 36(4), A1500–A1524.

Constantine, P. G., Emory, M., Larsson, J., & Iaccarino, G. (2015). Exploiting active subspaces to quantify uncertainty in the numerical simulation of the hyshot ii scramjet. *Journal of Computational Physics*, 302, 1–20. doi: 10.1016/j.jcp.2015.09.001

Constantine, P. G., Kent, C., & Bui-Thanh, T. (2016). Accelerating Markov chain Monte Carlo with Active Subspaces. *SIAM J. Sci. Comput.*, 38(5), A2779–A2805.

Cortesi, A., Constantine, P., Magin, T. E., & Congedo, P. M. (2017, August). *Forward and backward uncertainty quantification with active subspaces: application to hypersonic flows around a cylinder* (Research Report No. RR-9097). INRIA Bordeaux, équipe CARDAMOM. Retrieved from <https://hal.inria.fr/hal-01592591>

Hacker, P. (2003). Hydrologisch-hydrogeologische untersuchungen im bereich des glashüttenberges zur frage des engeren schutzgebietes für die kerschbaumerquelle. *ARC Seibersdorf research GmbH*.

Hartmann, A. (2018). Experiences in calibrating and evaluating lumped karst hydrological models. *Geological Society, London, Special Publications*, 466(1), 331–340. doi: 10.1144/SP466.18

Hartmann, A., Barberá, J. A., & Andreo, B. (2017). On the value of water quality data and informative flow states in karst modelling. *Hydrology and Earth System Sciences*, 21(12), 5971–5985. doi: 10.5194/hess-21-5971-2017

Hartmann, A., Barberá, J. A., Lange, J., Andreo, B., & Weiler, M. (2013). Progress in the hydrologic simulation of time variant recharge areas of karst systems – exemplified at a karst spring in southern spain. *Advances in Water Resources*, 54, 149–160. doi: 10.1016/j.advwatres.2013.01.010

Hartmann, A., Goldscheider, N., Wagener, T., Lange, J., & Weiler, M. (2014). Karst water resources in a changing world: Review of hydrological mod-

eling approaches. *Reviews of Geophysics*, 52(3), 218–242. doi: 10.1002/2013RG000443

Hartmann, A., Wagener, T., Rimmer, A., Lange, J., Brielmann, H., & Weiler, M. (2013). Testing the realism of model structures to identify karst system processes using water quality and quantity signatures. *Water Resources Research*, 49(6), 3345–3358. doi: 10.1002/wrcr.20229

Henson, W. R., de Rooij, R., & Graham, W. (2018). What makes a first-magnitude spring? - global sensitivity analysis of a speleogenesis model to gain insight into karst network and spring genesis. *Water Resources Research*. doi: 10.1029/2017WR021950

Hosseini, S. M., Ataie-Ashtiani, B., & Simmons, C. T. (2017). Spring hydrograph simulation of karstic aquifers: Impacts of variable recharge area, intermediate storage and memory effects. *Journal of Hydrology*, 552, 225–240. doi: 10.1016/j.jhydrol.2017.06.018

Jakeman, A. J., & Hornberger, G. M. (1993). How much complexity is warranted in a rainfall-runoff model? *Water Resources Research*, 29(8), 2637–2649. doi: 10.1029/93WR00877

Jefferson, J. L., Gilbert, J. M., Constantine, P. G., & Maxwell, R. M. (2015). Active subspaces for sensitivity analysis and dimension reduction of an integrated hydrologic model. *Computers & Geosciences*, 83, 127–138. doi: 10.1016/j.cageo.2015.07.001

Kitanidis, P. K., & Lee, J. (2014). Principal component geostatistical approach for large-dimensional inverse problems. *Water resources research*, 50(7), 5428–5443.

Koeck, R., & Hochbichler, E. (2012). Das wald-hydrotop-modell als wsms-werkzeug im quellenschongebiet der stadt waidhofen/ybbs. *Report in the course of the CC-WaterS project*.

Mazzilli, N., Jourde, H., Jacob, T., Guinot, V., Le Moigne, N., Boucher, M., ... Legtchenko, A. (2013). On the inclusion of ground-based gravity measurements to the calibration process of a global rainfall-discharge reservoir model: case of the durzon karst system (larzac, southern france). *Environmental Earth Sciences*, 68(6), 1631–1646. doi: 10.1007/s12665-012-1856-z

Moussu, F., Oudin, L., Plagnes, V., Mangin, A., & Bendjoudi, H. (2011). A multi-objective calibration framework for rainfall–discharge models applied to karst systems. *Journal of Hydrology*, 400(3-4), 364–376. doi: 10.1016/j.jhydrol.2011.01.047

Sheikhy Narany, T., Bittner, D., Disse, M., & Chiogna, G. (2018). Spatial and temporal heterogeneities in hydrochemistry of small scale karst environment. *Environmental Earth Sciences*(under review).

Tarantola, A. (2005). *Inverse problem theory and methods for model parameter estimation* (Vol. 89). siam.

Teixeira Parente, M., Mattis, S., Gupta, S., Deusner, C., & Wohlmuth, B. (2018). Efficient parameter estimation for a methane hydrate model with active subspaces. *arXiv preprint arXiv:1801.09499*.

Tritz, S., Guinot, V., & Jourde, H. (2011). Modelling the behaviour of a karst system catchment using non-linear hysteretic conceptual model. *Journal of Hydrology*, 397(3-4), 250–262. doi: 10.1016/j.jhydrol.2010.12.001